ENERGY TRANSPORT MECHANISMS AND THE EVENT OF 16^{TH} DECEMBER 1991

J. L. Culhane [1], A. T. Phillips [1], T. Kosugi [2], M. Inda-Koide [2], C. D. Pike [3]

[1] *Mullard Space Science Laboratory, University College London, Holmbury St. Mary, Dorking, Surrey, RH5 6NT, England*
[2] *Dept. of Physics, Faculty of Science, The University of Tokyo, Bunkyo-ku, Tokyo 113, Japan*
[3] *Rutherford Appleton Laboratory, Chilton, Didcot, OX11 0QX, U.K.*

Abstract

The flare of 16^{th} December 1991 had relatively simple structure, which has made it useful for studing the energetics of chromospheric evaporation. Energy balance calculations for this flare support an electron beam energy deposition hypothesis for this event. The creation of 'super-hot' plasma is also investigated, using YOHKOH Hard X-ray Telescope images. Contrary to previously reported events, the 'super-hot' plasma in the 16^{th} December flare is generated, and remains close to the chromospheric footpoints, with a decay time consistent with saturated thermal conduction to the chromosphere.

1. Introduction

The flare of 16^{th} December 1991 was a M2.7 class flare which occurred in Active Region 6961, at a heliocentric longitude of 45W, and was observed by the YOHKOH satellite (Ogawara *et al.* , 1991). As Soft X-ray Telescope data was not available for this flare, the flare morphology has been investigated using images constructed by the Maximum Entropy Method from Hard X-ray Telescope (HXT, Kosugi *et al.* , 1991) data.

2. Flare Structure

The Light curves for the Bragg Crystal Spectrometer (BCS, Culhane *et al.* , 1991) CaXIX channel (3.9 keV) and the HXT LO (14-23keV), M1 (23-33keV), and HI (53-93keV) bands are shown in Figure 1. The light curve of this event can be divided into two distinct phases, by time and by energy. The higher energy bands of the HXT (> 50 keV) register only an impulsive non-thermal burst, which occurs first, and is caused by thick-target electron

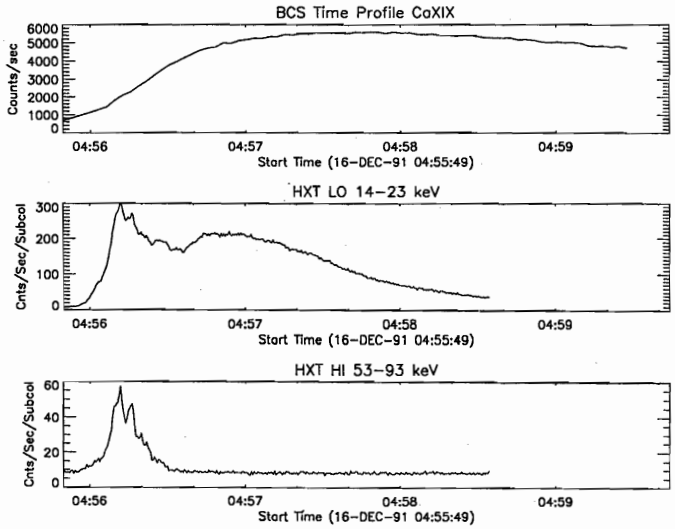

Fig. 1. HXT and BCS light curves for the event of 16^{th} December 1991. The HXT plots represent the average counting rates (with a 0.5 sec integration) of the 64 imaging elements of the HXT in counts/subcollimator/sec. The BCS time profile represents the counting rate derived from a 3 second integration. The 'background' present at the start of the CaXIX light curve is due to the decay of flare in another active region.

bremsstrahlung on the chromosphere. At lower energies (< 30 keV) significant thermal emission, following the impulsive burst can be seen. This thermal emission dominates the CaXIX channel of the BCS.

Images taken in the HI band show that the non-thermal emission is confined to two footpoints. Co-alignment of a pre-flare SXT image and the impulsive phase HI-band images suggest that these footpoints are those of a single small loop running N-S across a magnetic neutral line in the active region. Images from the LO band, shown in Figure 2., initially also show the footpoint emission, but as the flare evolution progresses past the impulsive burst to the peak of the softer thermal emission, the corresponding images show plasma emission moving out along an arc. At the peak of the gradual phase the loop is seen to be completely filled. The heated plasma then cools by conduction from the ends of the loop to the chromosphere.

Evidence for this single loop filling interpretation can be found in both the co-incidence of the Hard X-ray light curves for each footpoint, and in the temporal variation of the blue shifts observed in the CaXIX resonance line. Initially, during the impulsive phase and the first part of the gradual phase up to 04:57:00 UT, the blueshifted emission dominates, but this component rapidly fades, until, at 04:58 UT which is the peak of the CaXIX light curve, the blue shifted component to the resonance becomes insignificant, indicating that directed upflows have largely ceased at this time.

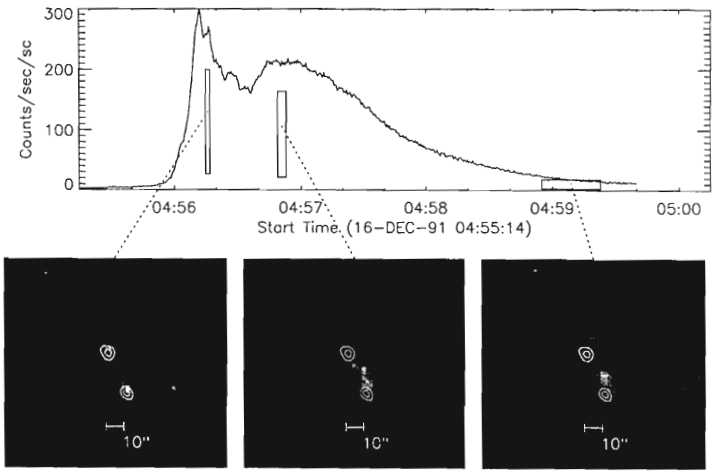

Fig. 2. HXT LO (14-23keV) band images. Image integration time is indicated by the width of the box on the light curve. FOV is 126" by 126", The contours shown are those of a HI (53-93keV) band image taken at 04:56:12 UT and represent 30, 60 and 90% of the peak intensity in that frame. All images were created using the MEM method. The intensity of each image is normalised to the peak of that frame for the purposes of display.

3. Energy Balance

This interpretation has also been quantiatively tested by performing an energy balance calculation, using a technique similar to that employed by Antonucci *et al.* 1982, on SMM data. The energy deposited by non-thermal electrons in the chromosphere was determined by fitting a power-law to HXT spectral observations, and inferring the energy deposited based on the assumption of a thick target Bremsstrahlung process (Hudson, Canfield and Kane 1978).

The energy contained in soft X-rays was calculated by fitting the CaXIX spectra using the method described by Fludra *et al.* 1989. This technique provides values of temperature and emission measure for the stationary plasma, and values of emission measure and average velocity for the upflowing plasma. These parameters were then used to calculate the thermal energy in the soft X-ray emitting plasma, and the losses by radiation and conduction for both stationary and upflowing plasma components. Thermal conduction to the chromosphere was found to be the most efficient loss process, accounting for 43% of the total thermal energy, whilst radiative losses accounted for only 3%.

The energy deposited by non-thermal electrons over the impulsive phase was calculated to be about 1×10^{30} ergs. The energy in the soft X-ray emitting material at the end of the evaporation phase was found to be 1.4×10^{30} ergs. These figures are of the same order of magnitude, and represent good agreement with the hypothesis of beam driven chromospheric evaporation.

A major criticsm of this type of energy balance calculation has been that of the small

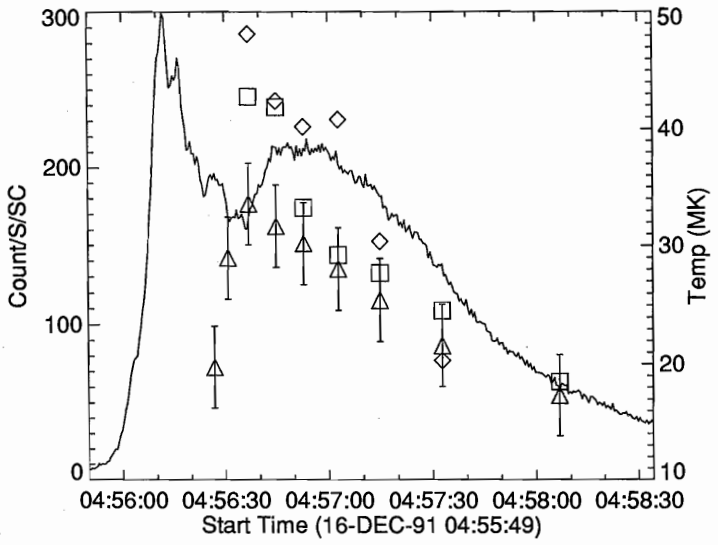

Fig. 3. Plasma Temperatures for loop footpoints and centre. Results of HXT thermal fits to three regions; each footpoint and the loop centre. The points are superimposed on an HXT LO band light curve, and are; Diamonds - North footpoint, Squares - South footpoint, Triangles - Loop centre. Error bars are shown for the loop centre points only, and represent a combined error of +/- 10% in both channels used in the temperature determination.

filling factors, of the order of a few percent, which were calculated for the flaring volumes (Wu *et al.* 1986). The increased spatial resolution of the Yohkoh instruments allows more confidence that the bounding volume calculated for the flaring plasma is closer to reality than was possible for earlier instruments, where spherical or cubical bounding volumes based on the instrumental or spatial resolution (Acton *et al.* 1982) have been used. Densities calculated for these volumes, based on emission from ions with emissivities peaking at temperatures in the region of 4×10^6K (Wolfson *et al.* , 1983) may also be subject to contamination from the surrounding active region plasmas, given recent reports of long-lived regions of high temperature (5×10^6K) in some non-flaring active regions (Hara *et al.* 1992). We therefore studied the temperature decay of the cooling CaXIX plasma, by fitting a conductive cooling curve to the fitted temperatures. The slope of the conductive loss curve, given by $\alpha = 1.2 \times 10^{10}/N_e \left(\frac{L}{2}\right)^2$ (Culhane, Vesecky and Phillips, 1970) is a function of the loop length and the electron density only. The electron density from the observed loop volume and emission measure was 2.5×10^{11} cm^{-3} , and that from the best-fit cooling curve was 3.6×10^{11} cm^{-3} . This gives an estimate for the filling factor of the loop of about 70%.

4. Super-Hot Component

The presence of a 'super-hot' plasma component during this solar flare was detected by both the BCS FeXXVI channel and by thermal fits to the lower energy HXT bands. This component has been seen by previous experiments (Lin *et al.* 1981, Tanaka 1987), and has

been conventionally sited near the top of the coronal loop.

Images taken in the HXT LO and M1 channels were used to determine the temperatures of three regions, surrounding each of the loop footpoints, and the loop centre, as a function of time. The results are shown in Figure 3., superimposed on the HXT LO channel light curve. The loop centre is consistently cooler than the footpoints. The loop footpoints show an elevated temperature, which persists for about 20-30 seconds. The localisation of the superhot plasma close to the chromosphere would indicate a classical thermal conduction lifetime on the order of a few seconds, but once the effect of conductive flux saturation (Karpen and DeVore 1987) is included, the calculated lifetime extends to 25 seconds, which is consistent with the observations.

5. Conclusions

This impulsive flare provides support for the chromospheric evaporation model, both morphologically and energetically. The filling factor associated with this event has been calculated, and supports the observed loop volume. The filling factor for this event is high compared to events studied by other instruments, which we attribute mainly to the improved spatial resolution of the YOHKOH instruments. This event also provides one of the few spatially resolved observations of superhot plasma. This plasma component is placed near the chromosphere, which together with the timing relative to the impulsive burst, implies a direct link between the generation of superhot plasma and the process of evaporation of chromospheric material.

Acknowledgments

We would like to acknowledge the support of ISAS, the UK SERC, and the British Council.

References

1. Acton L. W., Canfield, R. C., Gunkler, T. A., Hudson, H. S., Kiplinger, A. L., Leibacher, J. W., 1982 *Ap. J.*, **263**, 409
2. Antonucci, E., Gabriel, A. H., Acton, L. W., Culhane, J. L., Doyle, J. G., Leibacher, J. W., Machado, M. E., Orwig, L. E., Rapley, C. G., 1982 *Solar Phys.*, **78** 107
3. Culhane, J. L., Vesecky, J. F., Phillips, K. J. H., 1970 *Solar Phys.*, **15**, 394-413
4. Culhane, J. L., *et al.* , 1991 *Solar Phys.*, **136**, 89
5. Fludra, A., Lemen, J. R., Jakimiec, J., Bentley, R. D., Sylwester, J., 1989 *Ap. J.*, **344**, 991
6. Hara, H., Tsuneta, S., Lemen, J. R., Acton, L. W., McTiernan, J. M., 1992, *Publ. Astron. Soc. Japan*, **44**, L135
7. Hudson, H. S., Canfield, R. C., & Kane, S. R. 1978 *Solar Phys.*, **60**, 137
8. Karpen, J. T., DeVore, C. R., 1987 *Ap. J.*, **320**, 904
9. Kosugi, T., *et al.* , 1991 *Solar Phys.*, **136**, 17
10. Lin, R. P., Schwartz, R. A., Pelling, R. M., Hurley, K. C. 1981 *Ap. J.*, **251**, L109
11. Ogawara, Y., *et al.* , 1991 *Solar Phys.*, **136**, 1
12. Tanaka, K., 1987 *Publ. Astron. Soc. Japan*, **39**, 1
13. Wolfson C. J., Doyle, J. G., Leibacher, J. W., Phillips, K. J. H., 1983 *Ap. J.* , **269**, 319
14. Wu, S. T., *et al.* 1986, Energetic Phenomena on the Sun, ed. M. Kundu and B. Woodgate (NASA CP-2439), chap 5.